Published in final edited form as:

Dev Biol. 2016 April 01; 412(1): 32–43. doi:10.1016/j.ydbio.2016.02.016.

Lens placode planar cell polarity is dependent on Cdc42-mediated junctional contraction inhibition

Maria Muccioli[1], **Dalya Qaisi**[1], **Ken Herman**, **Timothy F. Plageman Jr.**[*]

College of Optometry, The Ohio State University, Columbus, OH 43210, United States

Abstract

Development of the ocular lens commences with the formation of the lens placode, an epithelial structure that thickens and subsequently bends inward in a process called invagination. Invagination is observed during the development of many embryonic structures, but the spectrum of morphogenetic events driving this process are, in most cases, not fully understood. A characteristic commonly found in embryonic tissues undergoing epithelial reorganization is planar polarity, a property where cells are geometrically and/or molecularly orientated in a specific direction along the plane of an epithelium. Planar polarity is known to drive the morphogenesis of several epithelial structures, however its role during invagination events is less clear. We have found that at the onset of invagination, cells of the lens placode become geometrically planar polarized such that they are orientated toward a central point in the lens placode. Further investigation revealed that this is due to contraction of radially orientated junctions and the elongation of those circumferentially orientated. Radial junctions have an elevated localization of actomyosin and their contraction is dependent on the F-actin and Rho-kinase binding protein, Shroom3. Elongation of circumferential junctions is dependent upon Cdc42, a Rho-GTPase known to regulate polarity via the Par-complex. We determined that Cdc42 and members of the Par-complex inhibit Shroom3-induced contractility and promote anisotropic placode cell geometry through inhibition of junctional contraction. We postulate that invagination of the lens placode requires careful orchestration of these opposing processes which are mediated by the planar polarization of junctional proteins.

1. Introduction

Epithelial tissue movements during embryogenesis are crucial to the generation of the three-dimensional shape of organs. One type of epithelial movement is invagination, a process where a plane of cells bends inward to form a depression or pit that often pinches off to form the primordium of a nascent organ. The early development of the pituitary, olfactory epithelium, thyroid, inner ear, and the retina all begin with epithelial invagination (Chauhan et al., 2015; Fagman and Nilsson, 2010; Fuhrmann, 2010; Jidigam and Gunhaga, 2013; Sai and Ladher, 2015; Scully and Rosenfeld, 2002). Perhaps the best characterized invagination

[*]Corresponding author.

[1]Contributed equally to this manuscript.

Appendix A. Supplementary material

Supplementary material associated with this article can be found in the online version at http://dx.doi.org/10.1016/j.ydbio.2016.02.016.

event is that of the lens placode (Chauhan et al., 2015). Lens invagination is immediately preceded by the formation of the lens placode, an elliptical region of elongating ectodermal cells lying adjacent to the underlying optic vesicle. In mice, placode formation occurs at E9.5 followed shortly by the initiation of invagination occurring from E9.75 to E10.0 in five stages (Supplemental Fig. 1) (Lang et al., 2014). By E11.0 the process has concluded and the lens placode will have converted from a planar structure to a spherical vesicle that has separated from the surface ectoderm.

Investigating the molecular mechanisms of invagination using the lens as a model system has yielded important insights. For example, apical constriction, a process consisting of the circumferential contraction of the adherens junctional complex (AJC) that produces wedge-shaped cells, is required for the proper shape and size of the early lens (Plageman et al., 2010). Contraction of the actomyosin cytoskeleton in lens pit cell AJC's requires RhoA, Rho-kinase (Rock), Shroom3, and p120-catenin which combine to organize components of the AJC, link actomyosin to cadherins, and phosphorylate and activate non-muscle myosin to ultimately reduce apical bicellular junctional length (Lang et al., 2014; Plageman et al., 2011, 2010). Although disruptive, ablation of any of these genes does not prevent invagination from occurring implicating additional contributing mechanisms. A role for the extracellular matrix and filopodia-like extensions from the lens to the optic vesicle have also been implicated but eliminating key extracellular matrix proteins or filopodia is still permissive for invagination to proceed (Chauhan et al., 2009; Huang et al., 2011). Although apical constriction and the extracellular matrix certainly contribute, the major driving force or the major combination of forces required for lens invagination has yet to be discovered.

Epithelia are also commonly shaped through planar polarized cell behaviors. Distinct from apical-basal polarity, planar polarity orients cell geometry or processes in a specific direction within a plane and is commonly observed in many epithelia undergoing morphogenesis (Wallingford, 2012). Tissue elongation, for example, can be accomplished through convergent extension, a process utilizing coordinated cell rearrangements that depend on protein localization to specific junctions (Tada and Heisenberg, 2012). During germband extension of *Drosophila* embryos, convergent extension is driven by the contraction of cell junctions orientated perpendicular to the direction of elongation. These junctions contract due to the preferential localization of Shroom3, Rock, and Myosin IIb (Fernandez-Gonzalez et al., 2009; Simoes Sde et al., 2010, 2014). Convergent extension movements in the developing neural epithelia of mouse embryos also depend on the planar polarized localization of these proteins (McGreevy et al., 2015; Nishimura and Takeichi, 2008; Williams et al., 2014). Because these proteins responsible for junctional contraction have also been linked to lens placode morphogenesis and their distribution patterns are indicative of planar cell polarity, an obvious next step is to investigate whether the lens placode is similarly organized.

In this manuscript, we report for the first time that cells of the peripheral lens placode are planar polarized both geometrically and molecularly. We found that the apical anisotropic geometry of lens placodal cells is generated by planar polarized contraction of junctions orientated parallel to the radius of the placode and elongation of perpendicularly orientated junctions. Proteins responsible for junctional contraction are localized to the shorter, radial

junctions. To investigate the mechanisms of junction elongation we tested the hypothesis that the Rho-GTPase, Cdc42, and members of the Par-complex facilitate elongation through the inhibition of actomyosin contractile proteins. Cdc42 is a known organizer of the Par-complex in several model systems (Elias et al., 2015; Joberty et al., 2000; Warner and Longmore, 2009; Welchman et al., 2007) and is required for planar polarity in vertebrate and invertebrate systems (Choi and Han, 2002; Eaton et al., 1996; Kieserman and Wallingford, 2009; Kirjavainen et al., 2015). Utilizing conditional deletion of the *Cdc42* gene in the lens placode, we found that junction elongation in placodal cells undergoing planar polarization requires Cdc42. Combined with experiments performed in cultured cells, we found that junctional contraction and the polarized distribution of proteins required for contraction is antagonized by Cdc42 and members of the Par-complex.

2. Materials and methods

2.1. Mouse line maintenance and embryo generation and isolation

The following mouse lines and genotyping protocols have been previously generated and reported: *Shroom3Gt*(*ROSA53*)*Sor/J* (*Shroom3*^{Gt}) (Hildebrand and Soriano, 1999), *Le-cre* (Ashery-Padan et al., 2000), *Cdh1tm1Cle/J* (*E-cadherin-mCFP*) (Snippert et al., 2010), *Cdc42*^{flox} (Chen et al., 2006). For fixed specimens, embryos were removed from the uterus after hysterectomy of timed mated, pregnant females, fixed in 4% paraformaldehyde and stored in PBS.

2.2. Embryo culture and time-lapse imaging

To visualize embryonic lens placodes in real-time, homozygous *E-cadherin-mCFP* embryos were dissected from the uterus at E9.75 (approximately ~2 pm) in pre-warmed (37 °C) cell culture media (DMEM), and cultured in a cover-slipped depression slide immersed in pre-warmed (37 °C) 75% rat serum (Harlan Harlan #Bt-4520), 25% embryonic media (DMEM without Phenol Red, 55 U/ml penicillin/streptomycin, 2.2 mM glutamax, 11 mM Hepes buffer). The depression slide and embryos were incubated in a climate controlled (37 °C, 5% CO_2, humidified) environmental chamber surrounding an inverted Nikon A1R confocal microscope. Images were acquired with a 60 × Plan Apo VC objective, a 405 nm laser (3.4%) at 1024 × 1024 resolution every 10 min for ~4 h with an approximate 11 μm z-range (step size 0.5 μm). For analysis, the . nd2 files were exported to .tif files and imported as .czi files for analysis with ZEN (Zeiss).

2.3. Whole-mount embryo and cell-culture immunolabeling and imaging

Fixed, whole embryos isolated from time-mated females (E9.75–E10.5) were rinsed twice in PBS and placed into 4% milk or 2% serum (in PBS) containing one or more of the following primary antibodies or fluorescent labels overnight at 4 °C with constant rocking: rabbit anti-β-catenin (1:500; Santa Cruz, sc-7199), mouse anti-β-catenin (1:500; BD Biosciences, 610153), rabbit anti-Shroom3 (1:500, generously provided by Jeff Hildebrand), rabbit anti-myosin IIb (1:5000; Covance, PRB445P), mouse anti-p120-catenin (1:200; BD Biosciences, 610133), rabbit anti-Cdc42 (11A11, Cell Signaling), rabbit anti-aPKC (Santa Cruz sc-216), Phalloidin 488 (1:1000; Invitrogen, A12379), and Hoechst 33342 (1:1000; Sigma, B-2261). For Shroom3, Cdc42, and aPKC labeling, embryos were subjected to antigen retrieval where

they were immersed in 100 mM Tris pH 9.0 and placed into a pressure cooker for 15 min prior to primary antibody incubation. Following three PBS rinses, embryos were subsequently incubated with the appropriate Alexa Fluor (Invitrogen) secondary antibodies conjugated with a 488 or 594 fluorophore at a 1:1000 dilution (in PBS with 4% milk or 2% serum) for 2–4 h under constant rocking. MDCK cells were fixed in 100% methanol for 5 min and the same staining procedure was followed using the additional antibodies mouse anti-Flag (1:500; Sigma, F1804), rabbit anti-Shroom3 (GenScript custom antibody, MKTPENLEEPSATPC, 1:500). Specimens were imaged using either a Zeiss Axio observer inverted microscope equipped with a wide-field fluorescent light source and 40 × Plan-Apochromat objective, or an upright Zeiss Axio observer LSM 700 confocal microscope utilizing 405, 488, and 555 lasers (2–5% power) and a 40 × EC Plan-Neofluar objective. Whole embryos were imaged at a 1024 × 1024 resolution with a *z*-range of 7–15 μm and step distances of 0.5 μm.

2.4. Cell culture and transfection

MDCK cells were cultured to ~30% confluency in Transwell dishes, transfected with 0.1–0.5 μg of the indicated vectors (Mirus), and fixed 48 h later. The vectors utilized for transfection include the following: pCS2-Shroom3-Flag (Plageman et al., 2010), pWPI-FLAG-hPRKCI (Luke McCaffrey, Addgene plasmid # 35387), pcDNATM3.1/V5-His TOPO-PKCi-K274W (Pedro Salas, Addgene plasmid # 55690) (Wald et al., 2008), pK-myc-Par3b (Ian Macara, Addgene plasmid # 19388) (Joberty et al., 2000), and pcDNA3-EGFP-Cdc42(wt) (Klaus Hahn, Addgene plasmid # 12599) (Nalbant et al., 2004). Transgenic cells were identified by either the presence of the GFP tag (Cdc42) or immunolabeling with an epitope tag (Shroom3, aPKC, DN-aPKC, Par3). Transwell membranes were cut away from the plastic support, immunolabeled as described above, and mounted on slides for imaging.

2.5. Morphometric analyses and statistics

Apical circumferential and radial cell dimensions were quantified from .czi files using Zen 2012 (blue edition, Zeiss). First, five concentric rings with defined radii at 50 μm intervals (50–250 μm) were drawn around the center of the placode. Using AJC labeling as guides, all cells lying on the circles were measured in two dimensions; the circumferential dimension was measured between the points its' junctions crossed the circles while the radial dimension was measured between the inner and outer junctions at a point approximately half-way and perpendicular to the first line. All measurements were compiled among multiple placodes (see Section 3 for the number of placodes analyzed) and averaged. Statistical comparisons were made between Stage 0 and Stage I at specific radial distances or between genotypes at a defined radial distance and stage using a *T*-test. Apical areas for placodal and MDCK cells were calculated using the spline contour tool on the ZEN software. The apical area was correlated with Cdc42 signal intensity using a recorded macro in ImageJ where the apical junctions of a cell was outlined and measured successively for area, then the average intensity along the line. 460 cells were measured from the central region of three Stage I placodes and divided into two groups by area. Statistical differences for every analysis were in all cases evaluated between two groups of data and were considered significant when the *p*-value was below 0.05.

To quantify contraction and elongation rate, 10 randomly chosen, circumferentially orientated elongating junctions, circumferentially contracting junctions and radially orientated junctions were measured at each 10 minute time point at the apical most point in the *z*-series using the graphics tools in the ZEN software. The difference of length for each junction between each 10 min time point (in ~4h) was found and the average change was compiled among all time points from each junction. For Fig. 3C and D, the data from 4/10 junctions are displayed.

Measuring the junctional orientation angle simultaneously with the intensity was accomplished by compiling 4–6, 50 μm square regions from confocal images of 3–6 placodes into a single . tif file such that their radial junctions were pointed toward the document's origin (top left corner) and analyzed with ImageJ. Using the line tool and measure function, all observable apical junctions not overexposed or obscured by staining inconsistencies were individually traced at their straightest point. The data gathered included the positional information of the line (X, Y, BY, BY) within the .tif document allowing for the angle to be calculated with Excel. Angle values were pooled and the average intensity of the junctions with angles that were within a specific angular range was determined. Statistical comparisons were made only between genotypes within a specific angular range using a *T*-test.

3. Results

3.1. Peripheral lens placodal cells become geometrically anisotropic at the onset of invagination

The major driving force for lens placode invagination has yet to be determined. In an attempt to ascertain novel aspects of this process we analyzed cell properties of fixed, whole-mounted embryos at multiple stages in this process with immuno-fluorescence rather than histological sections. Consistent with a previously defined lens invagination staging categorization (Lang et al., 2014), we have identified embryos that have a newly formed a lens placode (~E9.5) as Stage 0, and embryos with the first sign of invagination as Stage I (~9.75) (Fig. 1A, Supplementary Fig 1). Immunofluorescently labeling Stage 0 and Stage I embryos with a β-catenin antibody and analyzing the apical most junctions revealed a major alteration in the geometry of the cells. While cells of the central region of Stage 0 and Stage I lens placode within a 50 μm radius appeared roughly isometric (Fig. 1B′ and C′), the peripheral regions approximately 150–250 μm away from the placode center appeared anisotropic (Fig. 1B″ vs. C″) such that their circumferential lengths (the dimension perpendicular to the radius of the circular shaped placode) are longer than their radial lengths (the dimension parallel to the placodal radius). This apical cell geometry occurs 360° around the placode and the majority of cells are orientated toward a well-defined central point. Anisotropic apical cell geometry of peripheral lens placodal cells continues throughout invagination as evidenced by observing embryos with more advanced invagination (Fig. 1D; Stage II), and in the surface ectoderm at the fusion region of the lens pit during the conclusion of invagination (Fig. 1E; Stage V). In order to determine where anisotropic geometries occur and which dimensions change, we measured the circumferential and radial lengths of cells lying at increasing distances from the placode

center (Fig. 1F and G). We found that anisotropic geometry is generated by both an elongation of the circumferential length (Fig. 1F) and a decrease in the radial length (Fig. 1G). As expected, the changes in apical geometry are limited to the peripheral placodal cells and the central cells have similar circumferential and radial lengths (Fig. 1F and G).

Lens placodes from transgenic embryos expressing a fluorescently tagged (CFP) version of E-cadherin (Snippert et al., 2010) were also analyzed in real-time in order to visualize anisotropic geometry generation. Although measurement of static apical circumferential junctions from fixed specimens demonstrate that the average circumferential junction elongates, we found that this is not the case for all cells, and that some isotropically shorten their junctions (Fig. 2A, Movie 1). After quantifying and averaging the contraction rate of 10 radial and circumferential junctions over the course of 230 min (measured every 10 min) we found that junctional shortening rates between radial and circumferential junctions do not statistically differ (0.15 μm/min vs. 0.18 μm/min, respectively) (Fig. 2C). In agreement with our static measurements, these data demonstrate that anisotropic geometry is not generated by differential contraction rates. Analysis of the junctions from cells undergoing anisotropic geometry generation (Fig. 2B, Movie 2) revealed that junction elongation rates exceed that of junctional contraction (0.60 μm/min) (Fig. 2D) and that they can occur in the same cells simultaneously (arrowheads, Fig. 2B).

3.2. Proteins responsible for junctional contraction are planar polarized in peripheral lens placodal cells

Junctional contraction in the lens placode is dependent on the activation of non-muscle myosin which acts upon F-actin and requires the function of cytoskeletal and junctional proteins such as Shroom3 and p120 catenin. Upon analysis of whole-mount immunofluorescently labeled Stage I embryos we observed more intense immuno-labeling in the radial junctions (closed arrowheads) than circumferential junctions (open arrowheads) of peripheral but not central placodal cells when labeling for non-muscle myosin IIb (Myosin IIb) (Fig. 3A vs. B), F-actin (Fig. 3C vs.D), Shroom3 (Fig. 3E vs. F), and p120-catenin (Fig. 3G vs. H). To quantify these results, junctional intensity was simultaneously measured and compared with the junctional angle of incidence with respect to the placode radius (Fig. 3I). Junctions perpendicular to the placode radius have angle values close to 90° while those that were orientated more perpendicular have angle values nearing 180°. Unsurprisingly, the intensity values of Myosin IIb, F-actin, Shroom3, and p120-catenin mostly increase as the junctional angle approaches 180° (Fig. 3J) confirming our qualitative observations. In the case of Myosin IIb and p120-catenin the highest intensity value appears to occur in angles that are orientated slightly away (15–30°) from the circumferential direction. This may reflect the possibility that junctions that lie at this angle are more prone to junctional contraction.

We have previously demonstrated that Shroom3 is required for efficient isotropic apical junctional contraction in the lens placode. To determine if anisotropic geometry is similarly affected, we measured the circumferential and radial dimensions of Shroom3 deficient lens placodes (Fig. 3K and L). Unlike wild-type placodes, mutant placodal cells do not have anisotropic geometry and have circumferential:radial junction length ratios close to 1 (Fig.

3L and M). Compared with the Stage I measurements from Fig. 1F and G the 1:1 ratios in Shroom3 deficient cells are mostly due to the significantly longer than normal radial lengths in all measured regions (Fig. 3N). Circumferential length differences also occurred but varied from shorter to longer depending on the region measured. The failure of radial junction contraction in the absence of Shroom3 may be due to reduced activation of contractile actomyosin.

3.3. Anisotropic cell geometry and planar polarized protein localization is dependent upon Cdc42

As a known regulator of planar polarity and lens morphogenesis (Chauhan et al., 2009; Eaton et al., 1996), we next sought to determine if lens placode cell apical geometry is affected by the absence of Cdc42. When the Cdc42 gene is conditionally ablated from the lens placode using the *Le-cre* driver (Ashery-Padan et al., 2000), we observe that peripheral cells of Stage I lens placodes appear more isotropic (Fig. 4A and B). When the cell dimensions were measured and quantified from Stage 0 (n=4) and Stage I (n=6) control and mutant placodes we found that the circumferential to radial length ratios of peripheral cells (150–250 μm from center) are significantly reduced in Stage I embryos (Fig. 4C). Stage 0 mutant cells appear unaffected and like the control cells have isotropic apical areas (Fig. 4C). The ratio differences at Stage I are due to both a decrease in the average circumferential length and an increase in the average radial length of the apical cell areas (Fig. 4D). To visualize how the average dimensions affect cell geometry, the apical shape of cells were recreated using hexagons (due to placodal cells having ~5.8 neighbors) and calculated values, clearly demonstrating geometric differences (Fig. 4E). Circumferential shortening and radial elongation in mutant cells are consistent with a role for Cdc42 in promoting both circumferential junction elongation and radial junction contraction. We next determined how loss of Cdc42 affects the planar polarized localization of contractile proteins. Normally, there is quantifiably less Shroom3 protein observed in apical circumferential junctions of peripheral cells (Fig. 4F, arrowheads), but in Cdc42 deficient cells, Shroom3 protein localization in these junctions is more abundant (Fig. 4G, arrowheads). When junctional intensity was quantified and compared with the radial angle (quantified from 3 placodes), a significant reduction in the planar polarized localization of Shroom3 was apparent (Fig. 4H). Similar observations were made when immunolabeling control and mutant placodes for Myosin IIb (n=3) (Fig. 4I–J). The localization shift of the contractile inducing protein Shroom3 and Myosin IIb to circumferential junctions is consistent with the geometric changes where circumferential junctions become shorter; an occurrence possibly due to increased contractile activity. Likewise, radial junction elongation is potentially a result of reduced Shroom3 and Myosin IIb localization and therefore reduced contractility.

3.4. Cdc42 antagonizes isotropic junctional contraction

Rather than affect localization, another explanation for increased junctional contraction in the absence of Cdc42 is that it may antagonize the activity of contractile proteins. If this is the case we could expect to observe increased isotropic contractility in cells with isotropic localization of contractile proteins. To test this, we analyzed placodes from control and Cdc42 deficient embryos at Stage 0 where isotropic localization of Myosin IIb is observed (Fig. 5A–C). In the absence of Cdc42, the average apical area is significantly smaller at

Stage 0 in both central and peripheral cells (n=6 placodes) but not at Stage I (n=4 placodes) (Fig. 5A–C). Recreating the average circumferential and radial dimensions of Stage 0 cells from control and mutant placodes as hexagons (Fig. 5D) demonstrates the average size difference that occurs when Cdc42 is ablated.

To ascertain why Cdc42 ablation does not appear to affect isotropic contraction of central Stage I p we analyzed the localization of Cdc42 protein at this stage. Cdc42 is localized to the AJC in the lens placode (Fig. 5E and G) and much of the head surface ectoderm (Fig. 5F). Unlike the surface ectoderm where Cdc42 protein levels appear uniform in all cells, the central lens placode has patches of cells with reduced levels of Cdc42 protein in the AJC (n=3) (Fig. 5E, outlined region). Many of the cells with less Cdc42 protein (Fig. 5G, asterisks) appeared to have smaller apical areas than those with more Cdc42 (Fig. 5G, closed circles). When central placodal cells were simultaneously measured for AJC localized Cdc42 intensity and apical area, we found that cells larger than 25 μm^2 had significantly more Cdc42 protein in the AJC, than those with apical areas less than 25 μm^2 (Fig. 5H). These data are consistent with the possibility that Cdc42 protein localization to the AJC is dynamic and becomes reduced when cells isotropically contract their apical junctions. Together, decreased apical areas in Cdc42 mutant placodes and endogenous reduction of Cdc42 protein levels in smaller cells, point toward a role for Cdc42 in the inhibition of junctional contractility.

3.5. Cdc42 and members of the par complex inhibit Shroom3 mediated contractility in vitro

In order to confirm a role for Cdc42 contractile inhibition, we co-transfected plasmids containing Shroom3 with or without Cdc42 into MDCK cells, an epithelial cell line whose cells undergo apical junctional contraction in the presence of exogenous Shroom3 (Fig. 6A) (Hildebrand, 2005). In these cells, Shroom3 function can be quantitatively assessed by its ability to induce apical junctional contraction (Fig. 6A and I). MDCK cells transfected with control plasmids do not undergo apical junctional contraction (Fold change in apical area vs. untransfected cells=1.06) (Supplemental Fig. 2). Neither Cdc42 positive (Fig. 6B and I) nor Shroom3/Cdc42 positive MDCK cells (Fig. 6F and I) undergo apical junctional contraction, suggesting that Cdc42 can antagonize Shroom3 function. Because Cdc42 is known to be responsible for maintaining polarity through interactions with the Par-complex (Joberty et al., 2000), we tested whether Par3 or aPKC can similarly inhibit Shroom3 function. Interestingly, when expressed alone both Par3 and aPKC have cells with increased apical areas suggesting that they may antagonize endogenous AJC contractility activity (Fig. 6C,D and I). When expressed with Shroom3, both Par3 and aPKC significantly inhibit the ability of Shroom3 to induce apical junction contraction (Fig. 6G–I). Although aPKC significantly inhibited Shroom3 induced contractility, its ability to do so was less than that of Cdc42 (p<0.05). Because aPKC can anatagonize Rock activity via phosphorylation (Ishiuchi and Takeichi, 2011) and that Shroom3 induced junctional contraction is dependent upon Rock function (Hildebrand, 2005), we tested whether inhibiting aPKC activity can prevent Cdc42 from antagonizing Shroom3 function. Although apical areas and junctional contraction are unchanged in cells expressing both Shroom3 and Cdc42 (Fig. 6F), co-expression of a dominant negative version of aPKC significantly reduces apical areas and partially restores

Shroom3 dependent junctional contractility (Fig. 6E and I). These data suggest that aPKC function is required for Cdc42-dependent inhibition of Shroom3.

3.6. aPKC localization increases in radial junctions of Cdc42 deficient cells

Combined with the presented cell culture results, increased isotropic junctional contraction and reduced circumferential junctional length in Cdc42 deficient lens placode cells are all consistent with an inhibitory role for Cdc42 in junctional contraction. Left unexplained, is the increase in radial junctional length observed when Cdc42 is ablated. Given our result suggesting the requirement for aPKC function in this pathway, we analyzed its localization in peripheral Stage I lens placodal cells. Unexpectedly, we found that aPKC protein localization is planar polarized but elevated in radial vs. circumferential junctions (Fig. 7A and C). Upon analysis of aPKC localization in Cdc42 deficient lens placodes (n=3), we found that protein localization becomes significantly more associated with radial vs. circumferential junctions (Fig. 7B and C). The ability of aPKC to inhibit junctional contractility and its elevated abundance in radial junctions are consistent with the increase in radial junction length observed in Cdc42 deficient cells. Therefore, it is likely that radial junctional elongation could occur due to increased aPKC activity and reduced junctional contractility.

4. Discussion

4.1. Summary of results and conclusions

These results demonstrate for the first time that the lens placode and its constituent cells are both geometrically and molecularly planar polarized. The generation of anisotropic geometry of peripheral placodal cells occurs at the onset of invagination and a diagram of the hypothesized mechanism of planar polarity generation based on our principal findings is summarized in Fig. 8. We conceptualize the behavior of junctions as a balance between proteins promoting contractile function (Shroom3, Rock, Myosin IIb) and those antagonizing contraction which allow elongation (Cdc42, aPKC). In wild-type cells, proteins responsible for junctional contraction are found in greater abundance (localization levels represented by line thickness) in the AJC of junctions decreasing in length. Radial specific junctional contraction is at least partially responsible for generating anisotropic geometry of the cells as elimination of Shroom3 disturbs apical cell geometry (not depicted in Fig. 8). Although Cdc42 can anatogonize junctional contraction via aPKC and aPKC is found in greater amounts in radial junctions, we posit that the relative abundance and activity of contractile proteins outweigh that of the antagonizing activity. Conversely, we hypothesize that the lower abundance and activity of contractile proteins in circumferential junctions is outweighed by the antagonizing function of Cdc42 and aPKC and rather than contract, these junctions are permitted to elongate. In the absence of Cdc42, radial junctions are thought to lose their ability to contract owing to the increase in aPKC and decrease in Shroom3 and Myosin IIb localization and activity. We additionally hypothesize that the absence of Cdc42 causes circumferential junctions to contract due to increased contractile protein localization and decreased aPKC.

4.2. A potential role for anisotropic geometry generation during placode invagination

Although the deletion of several genes can perturb lens invagination, the process appears resilient and only completely fails when major signaling pathways, like the BMP pathway, are disrupted or essential transcription factors like Pax6 are ablated (Ashery-Padan et al., 2000; Jidigam et al., 2015; Rajagopal et al., 2009). For example, deleting genes important for junctional contraction or principal proteins of the extracellular matrix can disrupt the morphology of the lens, yet invagination still proceeds to varying degrees (Huang et al., 2011; Lang et al., 2014; Plageman et al., 2011, 2010). When Shroom3 is deleted, there is a reduction in apical constriction and efficient cell wedging (Plageman et al., 2010), but in many cases the lens placode still bends inward to a significant degree (Lang et al., 2014; Plageman et al., 2010) indicating that invagination is not simply regulated by apical constriction alone. The planar polarized nature of Shroom3-dependent junctional contractility observed in this study is an intriguing clue of an additional underlying mechanism.

A relevant attribute of the lens placode to this discussion is the increase in cell density that occurs at the onset of invagination (Hendrix et al., 1993). Because this cell density increase does not appear to be due to an elevated mitotic rate (Mckeehan, 1951; Zwaan and Pearce, 1971), it is conceivable that the combined effect of shortening radial junctions draws cells inward toward the center and causes the increase in cell density. The peripheral lens placode cells appear planar polarized throughout the entire invagination process suggesting that continual epithelial cell flow proceeds throughout invagination. We hypothesize that this radial epithelial cell flow may be a principal driver of lens placode invagination by forcing more cells into the central placode region. The placode may bend inward and perpendicular to the plane of the epithelium due to the central movement of cells much like Euler buckling of a sheet when a planar force is applied (Liu et al., 2015). In support of this hypothesis, *Shroom3* and *Cdc42* deficient mice have fewer cells in their invaginating lens placodes which could be due to inefficient anisotropic geometry generation (Chauhan et al., 2009; Plageman et al., 2010). Although Cdc42 mutant embryos have reduced anisotropic apical geometry, it is not wholly lost. Because invagination still occurs in *Cdc42* deficient embryos it is possible that additional molecules function redundantly with Cdc42 or with independent mechanisms. Additionally, the extracellular matrix or Cdc42-dependent filopodia that span the distance between the lens placode and optic vesicle may independently induce anisotropic geometry via more indirect mechanisms (Chauhan et al., 2009; Huang et al., 2011).

4.3. Mechanisms of junctional elongation

The mechanisms and purpose of junctional elongation during lens invagination are yet unclear. However, elongating junctions are observed in other examples of morphogenesis. For example, junction elongation is a hallmark of cell rearrangements that occur during germband extension in *Drosophila* and neural plate and kidney tubule elongation in mice (Blankenship et al., 2006; Lienkamp et al., 2012; Williams et al., 2014). In these tissues, cells rely on junctional elongation to resolve cellular rosettes during convergent extension which elongate epithelia (Harding et al., 2014). The lens placode surface area increases as the lens invaginates (Hendrix et al., 1993) and could be considered an elongating epithelia in

three dimensions. How elongation of cells around the lens placode perimeter affects the shape of the lens is a subject of our ongoing studies.

During *Drosophila* germband morphogenesis, junction formation and elongation is thought to depend on the sequential accumulation of F-actin, E-cadherin, and Bazooka, a homolog of the Par-complex protein Par3, to nascent junctions (Blankenship et al., 2006; Simoes Sde et al., 2010). Par-complex proteins may stabilize the adhesion between neighboring cellular membranes and permit elongation. Because Cdc42 regulates the activity of the Par-complex (Elias et al., 2015; Joberty et al., 2000; Warner and Longmore, 2009; Welchman et al., 2007), it is possible that Cdc42-dependent elongation of circumferential lens placode junctions similarly rely on Par-complex mediated adhesion.

In addition to promoting adhesion, an alternative or additional role for Cdc42 and the Par-complex is to antagonize junctional contractility. Similar to our results with *Cdc42*, *bazooka* mutants have reduced planar polarized localization of Myosin IIb in the junctions expected to contract (Simoes Sde et al., 2010). This reduced abundance may be indicative of reduced contractility. A more direct inhibitory role is observed in clonal knock-down experiments in *Drosophila* pupal eye epithelia, where junctional tension and apical area are dependent on Cdc42 (Warner and Longmore, 2009). These studies further showed that Cdc42 function is mediated by the Par-complex and aPKC, presumably through the phosphorylation and mislocalization of Rho-kinase (Ishiuchi and Takeichi, 2011; Warner and Longmore, 2009). Like circumferential junctions in the lens placode, Cdc42 reduction in the *Drosophila* eye also promoted an increase in junctional Myosin IIb (Warner and Longmore, 2009). Similarly, the Par-complex and the Ferm-domain containing protein, Willin, combine to inhibit Rho-kinase-dependent junctional contraction in cultured epithelial cells (Ishiuchi and Takeichi, 2011). Together with our studies, it is evident that the inhibition of junctional tension by Cdc42 and the Par-complex is evolutionarily conserved.

If downstream of Cdc42, it is unclear why aPKC did not affect Shroom3 induced contraction to the same degree as Cdc42. One possibility may be the endogenous protein abundance of Cdc42 vs. aPKC in MDCK cells. If endogenous Cdc42 levels are relatively low compared with aPKC in MDCK cells, then trasgenically expressed protein may differentially affect how Shroom3 is inhibited. It is also possible that Cdc42 may additionally affect pathways independent of aPKC that interfere with Shroom3 function.

Further characterization of the molecular mechanisms that regulate cellular junction remodeling within the lens placode will likely be required to discern the driving forces of invagination. Of particular interest are the signaling mechanisms regulating lens placode planar polarity generation. While members of the core-planar cell polarity are obvious candidates, many of these mutants do not have reported ocular or lens phenotypes suggesting a high level of functional redundancy during planar polarity generation (Murdoch et al., 2014; Torban et al., 2008; Wang et al., 2006). Although we cannot discount the participation of this pathway, additional signaling pathways could also be involved which are independent of the core planar cell polarity pathway and similar to what is observed in germband extension in *Drosophila* embryos (Pare et al., 2014; Zallen and Wieschaus, 2004). Future efforts will be focused on discerning the signaling pathways required to generate this

polarity and the continued use of live imaging will no doubt aid in determining the mechanisms of this morphogenetic event.

Supplementary Material

Refer to Web version on PubMed Central for supplementary material.

Acknowledgments

The authors would like to thank the March of Dimes Birth Defects Foundation (5-FY14-77) for funding, Sara Cole for her assistance with the live imaging experiments, and Richard Lang for providing mouse lines.

References

Ashery-Padan R, Marquardt T, Zhou X, Gruss P, 2000 Pax6 activity in the lens primordium is required for lens formation and for correct placement of a single retina in the eye. Genes. Dev 14, 2701–2711. [PubMed: 11069887]

Blankenship JT, Backovic ST, Sanny JS, Weitz O, Zallen JA, 2006 Multicellular rosette formation links planar cell polarity to tissue morphogenesis. Dev. Cell 11, 459–470. [PubMed: 17011486]

Chauhan B, Plageman T, Lou M, Lang R, 2015 Epithelial morphogenesis: the mouse eye as a model system. Curr. Top. Dev. Biol 111, 375–399. [PubMed: 25662266]

Chauhan BK, Disanza A, Choi SY, Faber SC, Lou M, Beggs HE, Scita G, Zheng Y, Lang RA, 2009 Cdc42- and IRSp53-dependent contractile filopodia tether presumptive lens and retina to coordinate epithelial invagination. Development 136, 3657–3667. [PubMed: 19820184]

Chen L, Liao G, Yang L, Campbell K, Nakafuku M, Kuan CY, Zheng Y, 2006 Cdc42 deficiency causes Sonic hedgehog-independent holoprosencephaly. Proc. Natl. Acad. Sci. USA 103, 16520–16525. [PubMed: 17050694]

Choi SC, Han JK, 2002 Xenopus Cdc42 regulates convergent extension movements during gastrulation through Wnt/Ca^{2+} signaling pathway. Dev. Biol 244, 342–357. [PubMed: 11944942]

Eaton S, Wepf R, Simons K, 1996 Roles for Rac1 and Cdc42 in planar polarization and hair outgrowth in the wing of Drosophila. J. Cell Biol 135, 1277–1289. [PubMed: 8947551]

Elias BC, Das A, Parekh DV, Mernaugh G, Adams R, Yang Z, Brakebusch C, Pozzi A, Marciano DK, Carroll TJ, Zent R, 2015 Cdc42 regulates epithelial cell polarity and cytoskeletal function during kidney tubule development. J. Cell Sci 128, 4293–4305. [PubMed: 26490995]

Fagman H, Nilsson M, 2010 Morphogenesis of the thyroid gland. Mol. Cell Endocrinol 323, 35–54. [PubMed: 20026174]

Fernandez-Gonzalez R, Simoes Sde M, Roper JC, Eaton S, Zallen JA, 2009 Myosin II dynamics are regulated by tension in intercalating cells. Dev. Cell 17, 736–743. [PubMed: 19879198]

Fuhrmann S, 2010 Eye morphogenesis and patterning of the optic vesicle. Curr.Top. Dev. Biol 93, 61–84. [PubMed: 20959163]

Harding MJ, McGraw HF, Nechiporuk A, 2014 The roles and regulation of multicellular rosette structures during morphogenesis. Development 141, 2549–2558. [PubMed: 24961796]

Hendrix R, Madras N, Johnson R, 1993 Growth pressure can drive early chick lens geometries. Dev. Dyn 196, 153–164. [PubMed: 8400401]

Hildebrand JD, 2005 Shroom regulates epithelial cell shape via the apical positioning of an actomyosin network. J. Cell Sci 118, 5191–5203. [PubMed: 16249236]

Hildebrand JD, Soriano P, 1999 Shroom, a PDZ domain-containing actin-binding protein, is required for neural tube morphogenesis in mice. Cell 99, 485–497. [PubMed: 10589677]

Huang J, Rajagopal R, Liu Y, Dattilo LK, Shaham O, Ashery-Padan R, Beebe DC, 2011 The mechanism of lens placode formation: a case of matrix-mediated morphogenesis. Dev. Biol 355, 32–42. [PubMed: 21540023]

Ishiuchi T, Takeichi M, 2011 Willin and Par3 cooperatively regulate epithelial apical constriction through aPKC-mediated ROCK phosphorylation. Nat. Cell Biol 13, 860–866. [PubMed: 21685893]

Jidigam VK, Gunhaga L, 2013 Development of cranial placodes: insights from studies in chick. Dev. Growth Differ 55, 79–95. [PubMed: 23278869]

Jidigam VK, Srinivasan RC, Patthey C, Gunhaga L, 2015 Apical constriction and epithelial invagination are regulated by BMP activity. Biol. Open 4, 1782–1791. [PubMed: 26621830]

Joberty G, Petersen C, Gao L, Macara IG, 2000 The cell-polarity protein Par6 links Par3 and atypical protein kinase C to Cdc42. Nat. Cell Biol 2, 531–539. [PubMed: 10934474]

Kieserman EK, Wallingford JB, 2009 In vivo imaging reveals a role for Cdc42 in spindle positioning and planar orientation of cell divisions during vertebrate neural tube closure. J. Cell Sci 122, 2481–2490. [PubMed: 19549689]

Kirjavainen A, Laos M, Anttonen T, Pirvola U, 2015 The Rho GTPase Cdc42 regulates hair cell planar polarity and cellular patterning in the developing cochlea. Biol. Open 4, 516–526. [PubMed: 25770185]

Lang RA, Herman K, Reynolds AB, Hildebrand JD, Plageman TF Jr., 2014 p120-catenin-dependent junctional recruitment of Shroom3 is required for apical constriction during lens pit morphogenesis. Development 141, 3177–3187. [PubMed: 25038041]

Lienkamp SS, Liu K, Karner CM, Carroll TJ, Ronneberger O, Wallingford JB, Walz G, 2012 Vertebrate kidney tubules elongate using a planar cell polarity-dependent, rosette-based mechanism of convergent extension. Nat. Genet 44, 1382–1387. [PubMed: 23143599]

Liu X, Wang F, Wu H, 2015 Anisotropic growth of buckling-driven wrinkles in graphene monolayer. Nanotechnology 26, 065701. [PubMed: 25597449]

McGreevy EM, Vijayraghavan D, Davidson LA, Hildebrand JD, 2015 Shroom3 functions downstream of planar cell polarity to regulate myosin II distribution and cellular organization during neural tube closure. Biol. Open 4, 186–196. [PubMed: 25596276]

Mckeehan MS, 1951 Cytological aspects of embryonic lens induction in the chick. J Exp. Zool 117, 31–64.

Murdoch JN, Damrau C, Paudyal A, Bogani D, Wells S, Greene ND, Stanier P, Copp AJ, 2014 Genetic interactions between planar cell polarity genes cause diverse neural tube defects in mice. Dis. Model. Mech 7, 1153–1163. [PubMed: 25128525]

Nalbant P, Hodgson L, Kraynov V, Toutchkine A, Hahn KM, 2004 Activation of endogenous Cdc42 visualized in living cells. Science 305, 1615–1619. [PubMed: 15361624]

Nishimura T, Takeichi M, 2008 Shroom3-mediated recruitment of Rho kinases to the apical cell junctions regulates epithelial and neuroepithelial planar remodeling. Development 135, 1493–1502. [PubMed: 18339671]

Pare AC, Vichas A, Fincher CT, Mirman Z, Farrell DL, Mainieri A, Zallen JA, 2014 A positional Toll receptor code directs convergent extension in Drosophila. Nature 515, 523–527. [PubMed: 25363762]

Plageman TF Jr., Chauhan BK, Yang C, Jaudon F, Shang X, Zheng Y, Lou M, Debant A, Hildebrand JD, Lang RA, 2011 A Trio-RhoA-Shroom3 pathway is required for apical constriction and epithelial invagination. Development 138, 5177–5188. [PubMed: 22031541]

Plageman TF Jr., Chung MI, Lou M, Smith AN, Hildebrand JD, Wallingford JB, Lang RA, 2010 Pax6-dependent Shroom3 expression regulates apical constriction during lens placode invagination. Development 137, 405–415. [PubMed: 20081189]

Rajagopal R, Huang J, Dattilo LK, Kaartinen V, Mishina Y, Deng CX, Umans L, Zwijsen A, Roberts AB, Beebe DC, 2009 The type I BMP receptors, Bmpr1a and Acvr1, activate multiple signaling pathways to regulate lens formation. Dev. Biol 335, 305–316. [PubMed: 19733164]

Sai X, Ladher RK, 2015 Early steps in inner ear development: induction and morphogenesis of the otic placode. Front. Pharmacol 6, 19. [PubMed: 25713536]

Scully KM, Rosenfeld MG, 2002 Pituitary development: regulatory codes in mammalian organogenesis. Science 295, 2231–2235. [PubMed: 11910101]

Simoes Sde M, Blankenship JT, Weitz O, Farrell DL, Tamada M, Fernandez-Gonzalez R, Zallen JA, 2010 Rho-kinase directs Bazooka/Par-3 planar polarity during Drosophila axis elongation. Dev. Cell 19, 377–388. [PubMed: 20833361]

Simoes Sde M, Mainieri A, Zallen JA, 2014 Rho GTPase and Shroom direct planar polarized actomyosin contractility during convergent extension. J. Cell Biol 204, 575–589. [PubMed: 24535826]

Snippert HJ, van der Flier LG, Sato T, van Es JH, van den Born M, Kroon-Veenboer C, Barker N, Klein AM, van Rheenen J, Simons BD, Clevers H, 2010 Intestinal crypt homeostasis results from neutral competition between symmetrically dividing Lgr5 stem cells. Cell 143, 134–144. [PubMed: 20887898]

Tada M, Heisenberg CP, 2012 Convergent extension: using collective cell migration and cell intercalation to shape embryos. Development 139, 3897–3904. [PubMed: 23048180]

Torban E, Patenaude AM, Leclerc S, Rakowiecki S, Gauthier S, Andelfinger G, Epstein DJ, Gros P, 2008 Genetic interaction between members of the Vangl family causes neural tube defects in mice. Proc. Natl. Acad. Sci. USA 105, 3449–3454. [PubMed: 18296642]

Wald FA, Oriolo AS, Mashukova A, Fregien NL, Langshaw AH, Salas PJ, 2008 Atypical protein kinase C (iota) activates ezrin in the apical domain of intestinal epithelial cells. J. Cell Sci 121, 644–654. [PubMed: 18270268]

Wallingford JB, 2012 Planar cell polarity and the developmental control of cell behavior in vertebrate embryos. Annu. Rev. Cell Dev. Biol 28, 627–653. [PubMed: 22905955]

Wang Y, Guo N, Nathans J, 2006 The role of Frizzled3 and Frizzled6 in neural tube closure and in the planar polarity of inner-ear sensory hair cells. J. Neurosci 26, 2147–2156. [PubMed: 16495441]

Warner SJ, Longmore GD, 2009 Cdc42 antagonizes Rho1 activity at adherens junctions to limit epithelial cell apical tension. J. Cell Biol 187, 119–133. [PubMed: 19805632]

Welchman DP, Mathies LD, Ahringer J, 2007 Similar requirements for CDC-42 and the PAR-3/PAR-6/PKC-3 complex in diverse cell types. Dev. Biol 305, 347–357. [PubMed: 17383625]

Williams M, Yen W, Lu X, Sutherland A, 2014 Distinct apical and basolateral mechanisms drive planar cell polarity-dependent convergent extension of the mouse neural plate. Dev. Cell 29, 34–46. [PubMed: 24703875]

Zallen JA, Wieschaus E, 2004 Patterned gene expression directs bipolar planar polarity in Drosophila. Dev. Cell 6, 343–355. [PubMed: 15030758]

Zwaan J, Pearce TL, 1971 Cell population kinetics in the chicken lens primordium during and shortly after its contact with the optic cup. Dev. Biol 25, 96–118. [PubMed: 5557971]

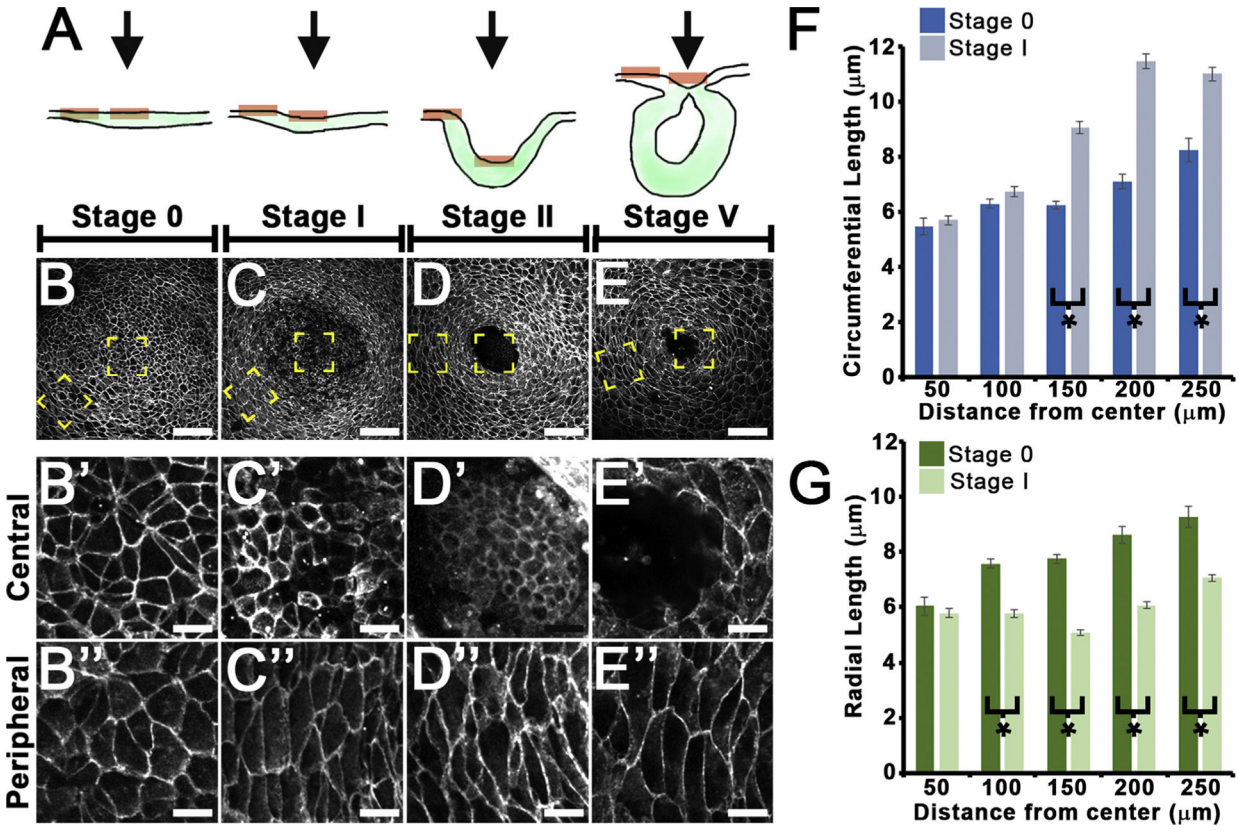

Fig. 1.

(A) Drawings of cross-sections of the corresponding lens invagination stages. The red boxes indicate the region magnified in (B′–E″) (B–E) β-catenin immunofluorescent labeling of whole-mount wild-type mouse embryos at four distinct lens invagination stages. The yellow squared region are magnified in the panels below. Note that the central region of Stage II/V placodes are out of the focal plane. Scale bars=50 μm (B–E); 10 μm (B′–E″). (F, G). The average apical length of cells measured in their circumferential (F) or radial dimensions (G) at five distances from the center of the placode at Stage 0 and Stage I. For the peripheral images, the placode center is to the right of the image. Note that the peripheral cell geometries become anisotropic at Stage I. Error bars show the standard error and the asterisks indicate $p<0.05$.

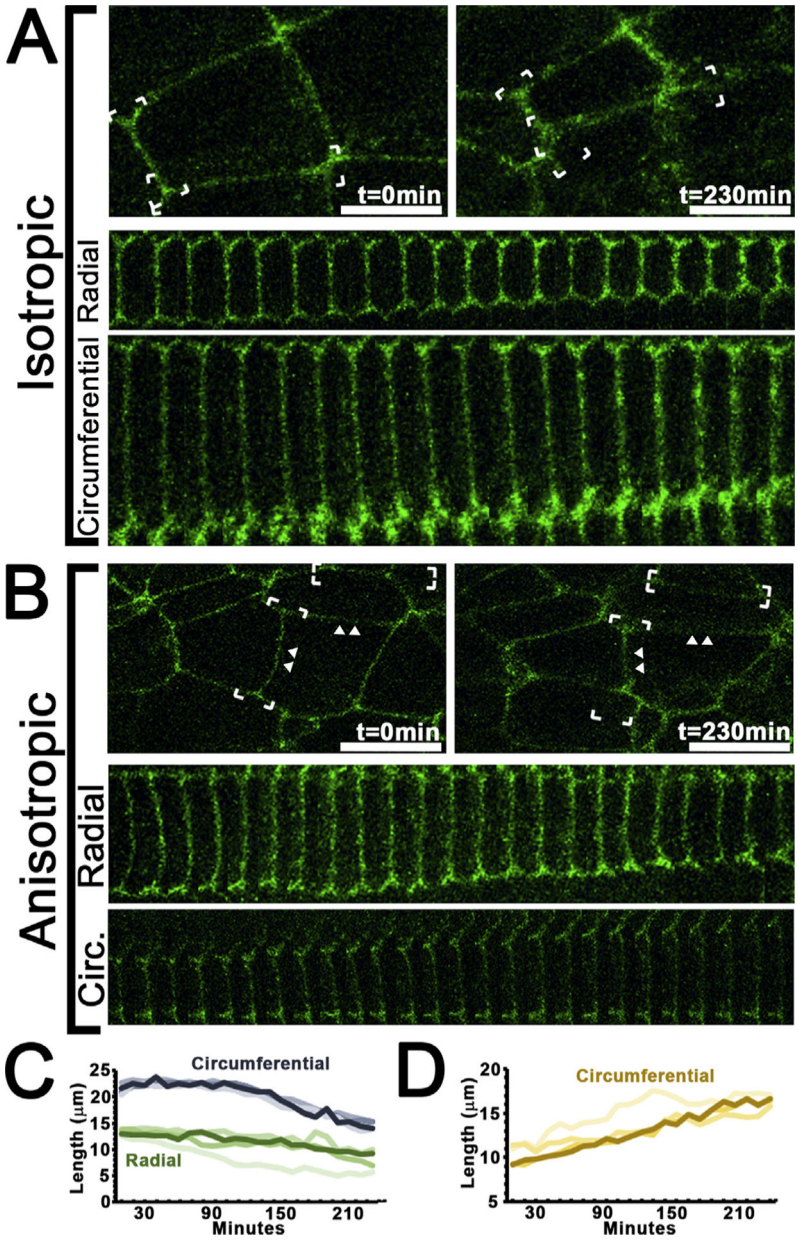

Fig. 2.

(A, B) Still images from movies of lens placode cells from *Ecad-mCFP* transgenic embryos changing their apical geometries. Cells are depicted that contract isotropically where both radially and circumferentially orientated junctions shorten (A), or cells contract their radial junctions but elongate their circumferential junctions (B). The top panels show two time-points of cells changing their apical shape (radial=up/down; circumferential=left/right), while the bottom two panels are an aggregate of images of specific junctions changing over the course of several frames (10 min intervals). White brackets indicate the junctions magnified in the bottom panels, and the scale bar=10 μm. (C, D). A graph of the measurements of the length of four apical or circumferential junctions contracting (C), or four circumferential junctions elongating (D) over the imaging time period.

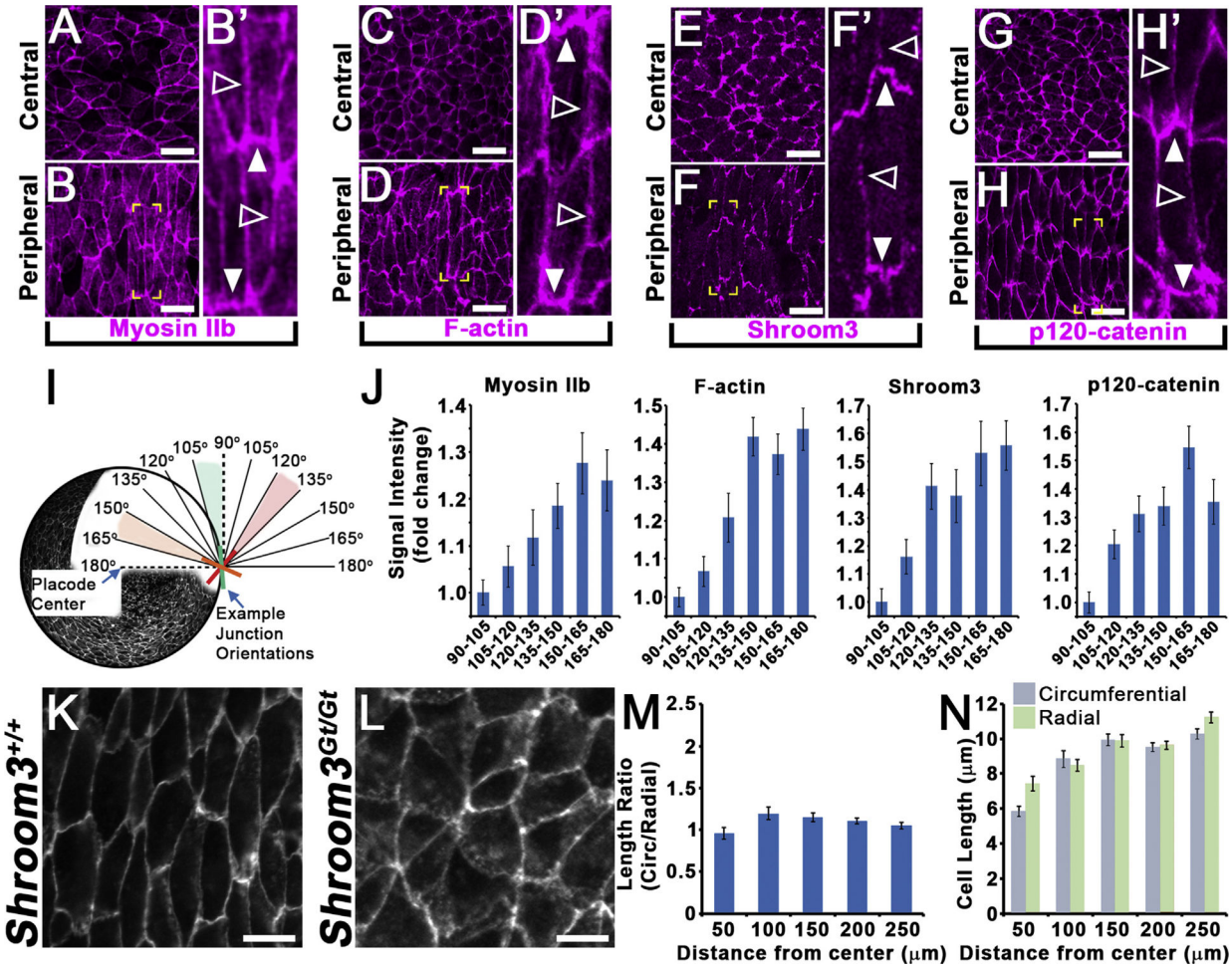

Fig. 3.

(A–H) Apical view of whole-mounted lens placodes immunofluorescently labeled for Myosin IIb (A–B), Phalloidin (C–D), Shroom3 (E–F), or p120-catenin (G–H). The images are taken of either the center of the placode (A,C,E,G) or 150–200 μm away from the center (peripheral, B,D,F,H). Closed and open arrowheads indicate radially or circumferentially orientated junctions, respectively. The yellow brackets indicate the regions magnified in B′–H′. (I) A depiction of how lens placode junction angles were measured for the following intensity measurements. (J) The graphs indicate the average intensity of immunofluorescent labeling simultaneously measured with the junctional angle with respect to the placodal radius. Note that as the angle increases, and is more radially orientated, the greater the junctional intensity. (K,L) Representative regions of the peripheral lens placode 150–200 μm away from the center of wild-type (K) or Shroom3 deficient (L) embryos immunofluorescently labeled with β-catenin. The placode center is orientated to the right of the images. (M, N) The graphs depict the average dimension ratios (M) and circumferential and radial length (N) of placodal cells from *Shroom3*$^{Gt/Gt}$ mutant embryos at five different distances from the placode center. Error bars represent the standard error and scale bars=10 μm.

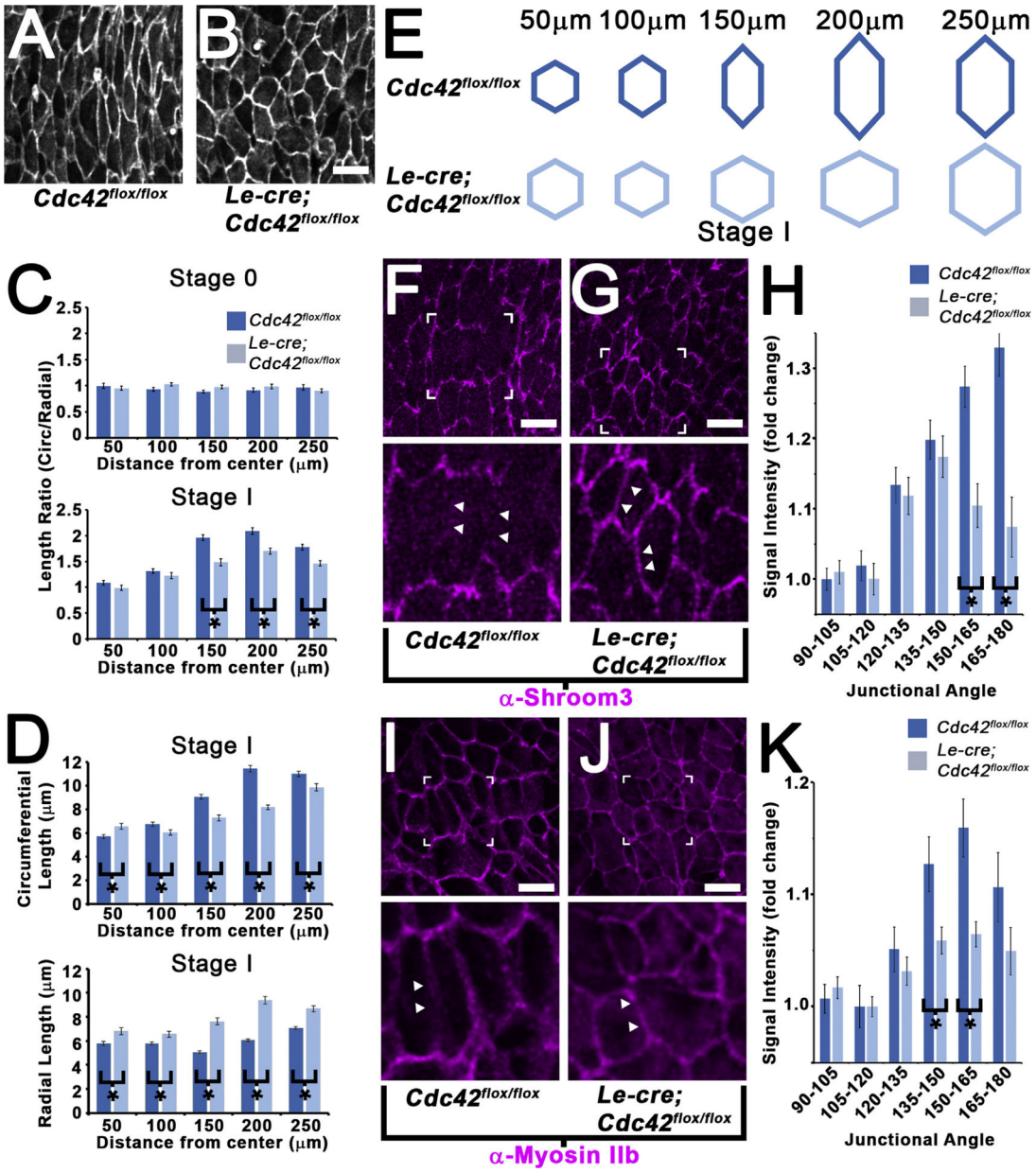

Fig. 4.

(A, B) Representative regions of the peripheral lens placode 150–200 μm away from the center of wild-type (a) or *Cdc42* deficient (B) embryos immunofluorescently labeled for β-catenin. (C) The graphs depict the average dimension ratios of cells from control or *Cdc42* mutant placodes at Stage 0 and Stage I located at the indicated distance from the center. Note that differences are not observed until Stage I. (D) The graphs depict the average circumferential and radial length of placodal cells from *Cdc42* mutant embryos located at the indicated distances from the placode center at Stage I. (E) The average cell dimensions from control and mutant placodes at the indicated distance from center were used to shape hexagons to model the average shape of cells in distinct placodal regions from different genotypes. (F–K) Representative regions from the placodes of control or *Cdc42* mutant

whole mounted embryos immunofluorescently labeled for Shroom3 (F, G) or Myosin IIb (I, J). Arrowheads indicate circumferentially orientated junctions, and the white bracketed region is magnified in the lower panels. The graphs (H, K) indicate the average intensity of immunofluorescent labeling simultaneously measured with the junctional angle with respect to the placodal radius. Note that the more radial measurements show significant differences in junctional intensity of both Shroom3 and Myosin IIb. Placode centers are orientated to the right of all images. Error bars represent the standard error, the scale bars=10 μm, and the asterisks indicate $p<0.05$.

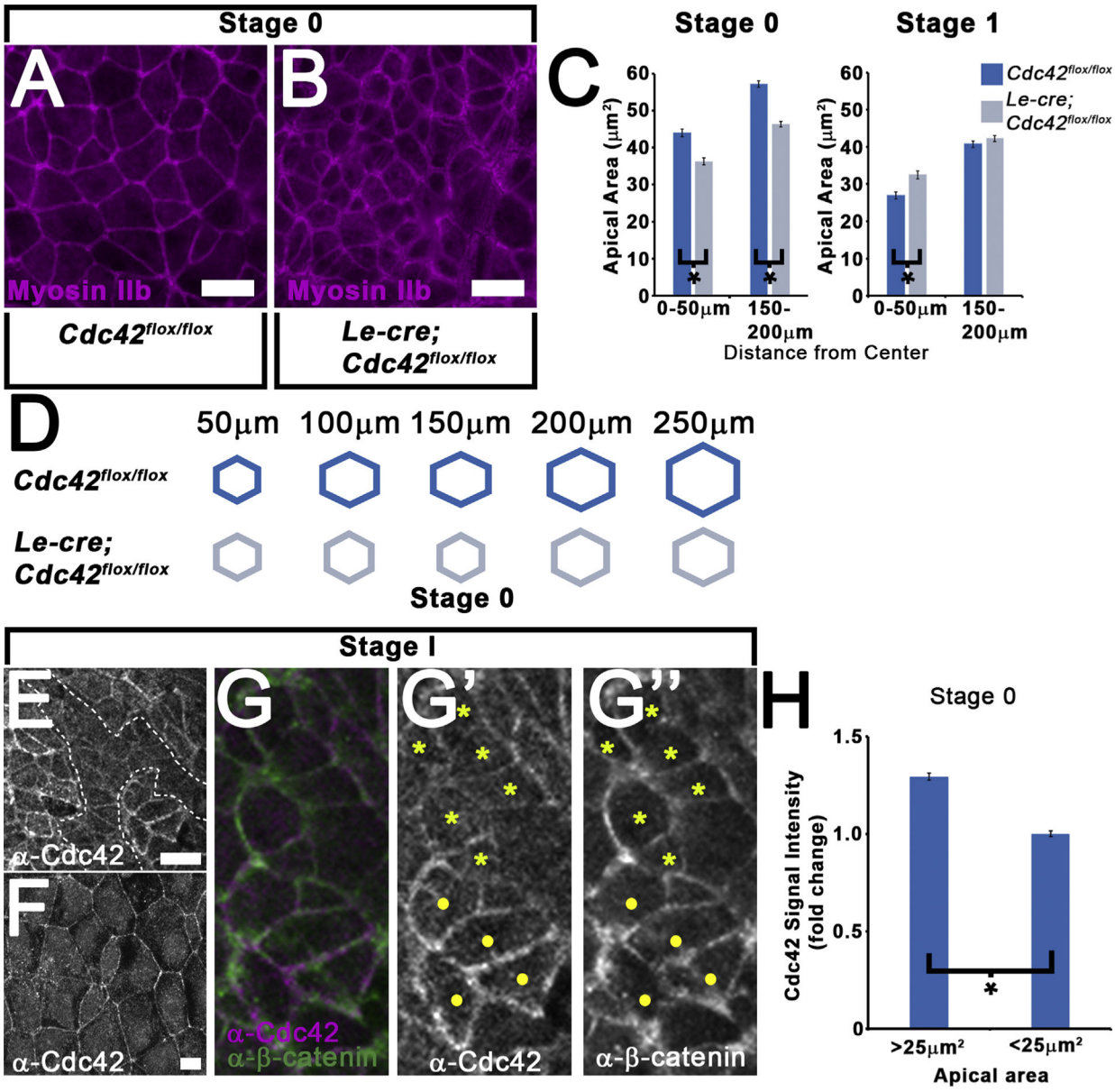

Fig. 5.

(A, B) Representative regions of the central lens placode of wild-type (A) or Cdc42 deficient (B) embryos immunofluorescently labeled for Myosin IIb. (C) The graphs depict the average apical area of cells within a 50 μm of the placode center or 150–200 μm away from the placode center at Stage 0 and Stage I. (D) The average cell dimensions from control and mutant Stage 0 placodes at the indicated distance from center were used to shape hexagons to model the average shape of cells in distinct placodal regions from different genotypes. Note that the apical areas are smaller in the absence of *Cdc42*. (E, F) Representative regions of the central lens placode (E) or surface head ectoderm (F) from whole-mounted wild-type embryos immunofluorently labeled for Cdc42. The bracketed area of E indicates a representative region of central placodal cells with lower junctional Cdc42 localization. (G) A magnified view of a portion of the region depicted in panel E showing co-labeling of

Cdc42 and β-catenin. The yellow circles and asterisks mark cells with high or low levels of junctional Cdc42, respectively. (H) The graph depicts the average junctional intensity of central placodal cells with apical areas less or greater than 25 μm^2. Note, that the junctional intensity is significantly reduced in cells with cells with smaller apical areas. Error bars represent the standard error, the scale bars=10 μ, and the black asterisks indicate $p<0.05$.

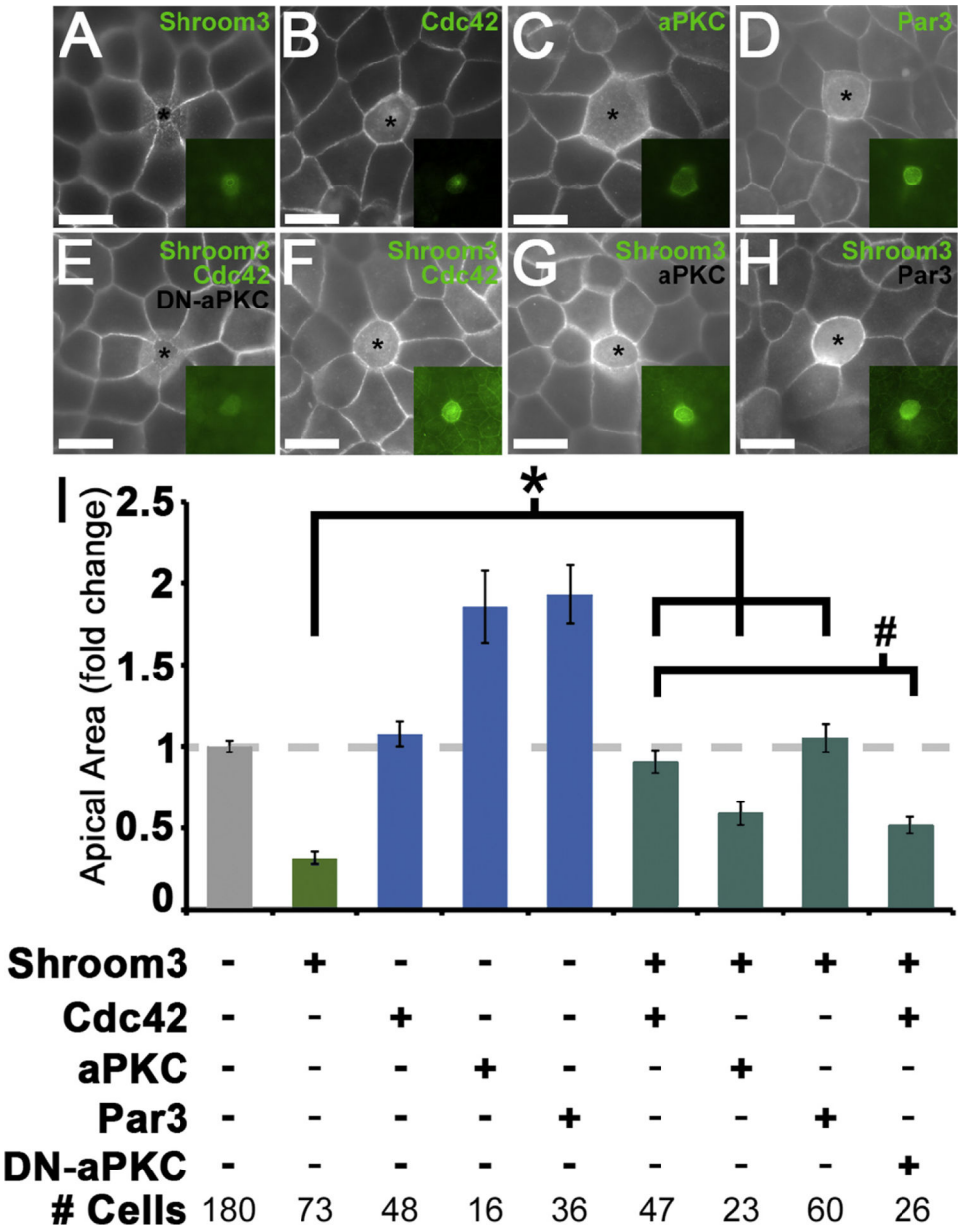

Fig. 6.

(A–H) Apical view of representative transgenic MDCK cells (asterisks) expressing the indicated plasmids immunofluorescently labeled for β-catenin (white) and the indicated transgene (green, inset). (I) The graph depicts comparisons between the average apical area of cells transfected with distinct combinations of indicated plasmids. The number of cells quantified for each group are listed below. The asterisk and pound-sign indicate averages that are significantly distinct from Shroom3 transfected cells or Shroom3 and Cdc42 co-transfected cells, respectively. Error bars represent the standard error, the scale bars=10 μm, and the black asterisks indicate $p<0.05$.

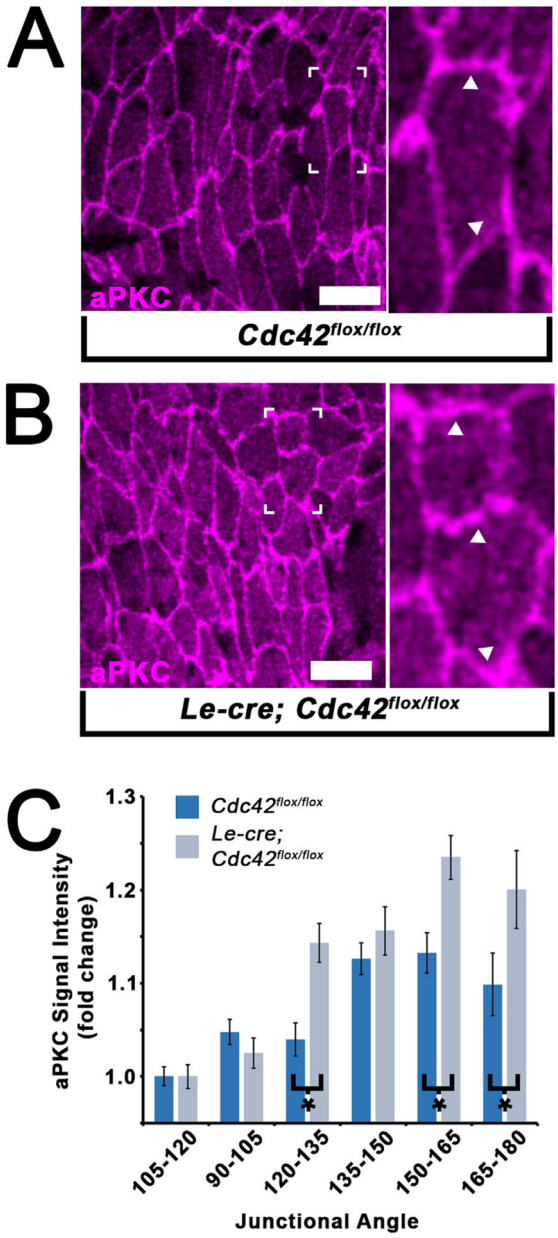

Fig. 7.

(A, B) Representative regions of the peripheral lens placode 150–200 μm away from the center of Stage I wild-type (A) or *Cdc42* deficient (B) embryos immunofluorescently labeled for aPKC. The white bracketed region is magnified to the right and arrowheads point out radial junctions. The scale bar=10 μm and the placode centers are orientated to the right of the images. (C) The graph depicts the average intensity of immunofluorescent labeling of junctional aPKC simultaneously measured with the junctional angle with respect to the placodal radius. Note that the more radial measurements show significant increases in junctional intensity for aPKC. Error bars represent the standard error, and the asterisks indicate $p<0.05$.

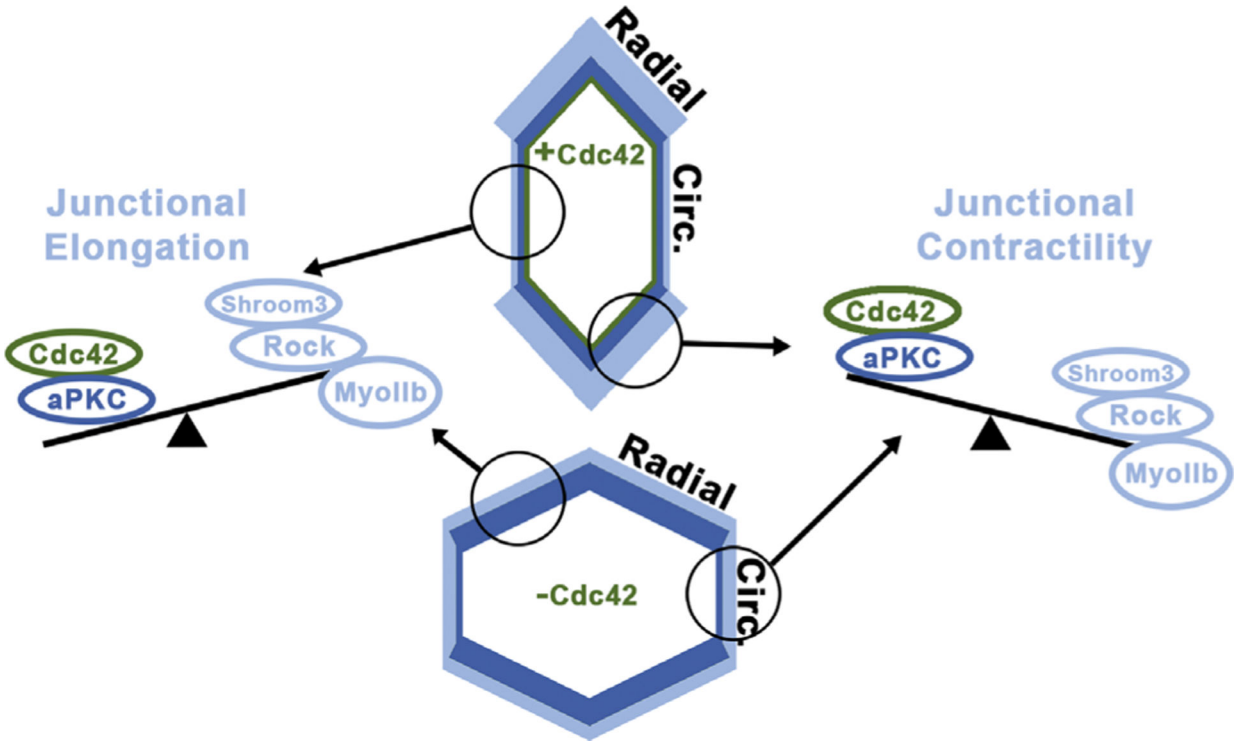

Fig. 8.

The average apical cell shape of Stage I wild-type and Cdc42 deficient peripheral cells are modeled here along with an exaggerated depiction of the relative localization of the color-matched junctional proteins, where the line thickness correlates with greater abundance. Junctional contraction is thought to occur when the sum of junctional contraction protein (Shroom3, Rock, Myosin IIb) activity conceptually outweighs that of the inhibitory proteins (Cdc42 and aPKC). Junctional elongation is thought to be permitted when the activity of the inhibitory proteins conceptually outweigh that of the contractility function. See the discussion for a full description.

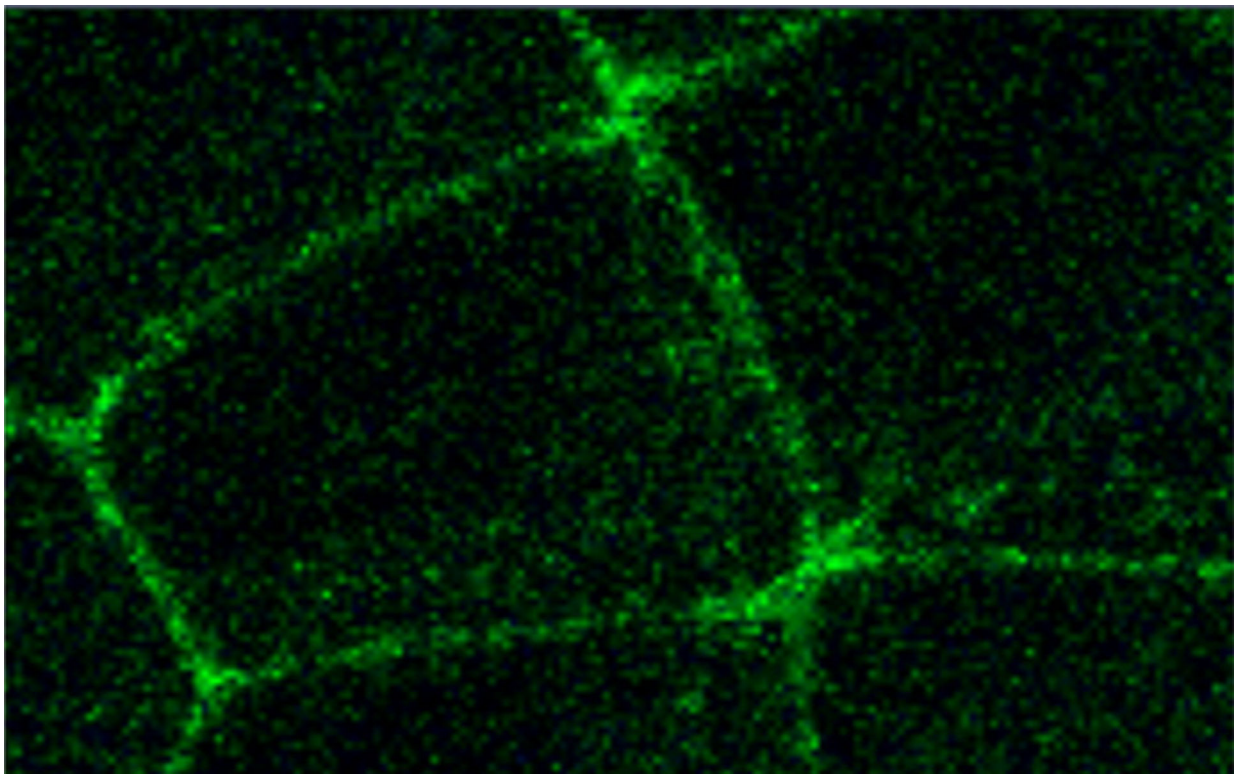

Movie 1.

Apical view of a placode cell from a *Ecad-mCFP* transgenic embryo over the course of 230 min (each frame is 10 min). Note that in this cell, junctional contraction occurs in both circumferentially (aligned left to right) and radially (aligned up and down) orientated junctions with respect to the placode center. A video clip is available online.Supplementary material related to this article can be found online at http://dx.doi.org/10.1016/j.ydbio.2016.02.016.

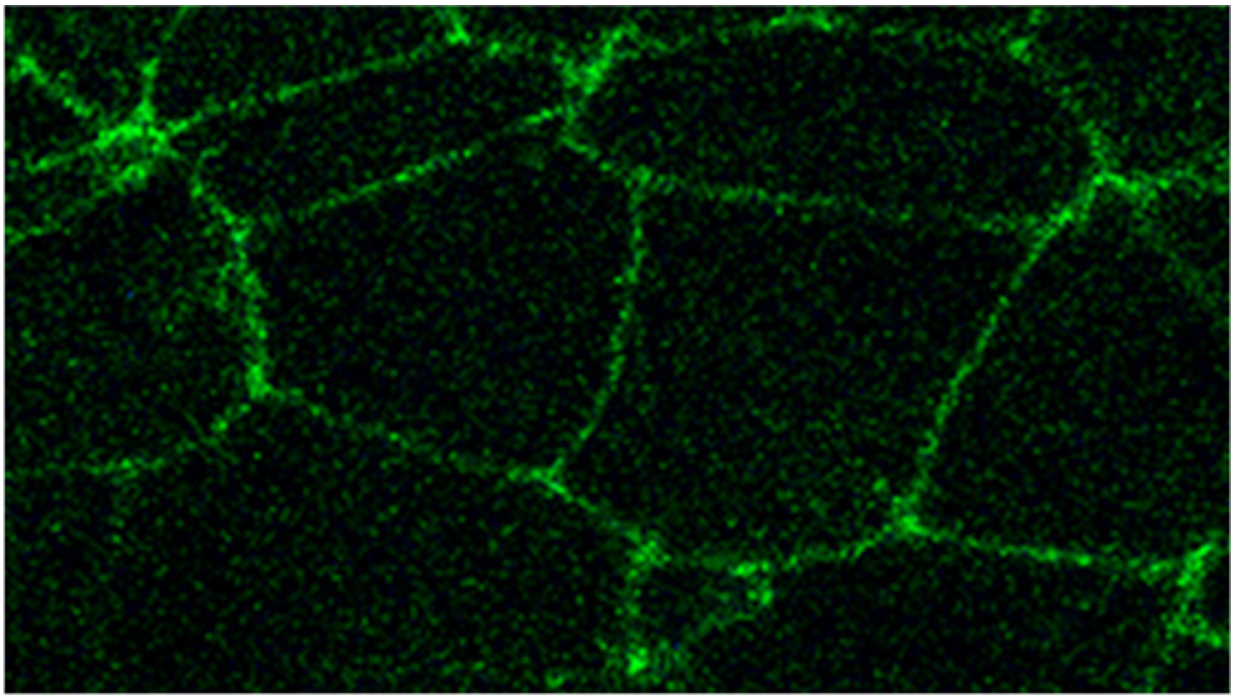

Movie 2.

Apical view of a group of placode cells from a *Ecad-mCFP* transgenic embryo over the course of 230 min (each frame is 10 min). Note that in these cells, junctional contraction occurs in radially orientated junctions (aligned top to bottom), while elongation occurs in those orientated circumferentially (aligned left to right).Supplementary material related to this article can be found online at http://dx.doi.org/10.1016/j.ydbio.2016.02.016.